PCCP- Electronic Supplementary Information

Electron scattering in large water clusters from photoelectron imaging with high harmonic radiation†

Thomas E. Gartmann‡, Sebastian Hartweg‡, Loren Ban, Egor Chasovskikh, Bruce L. Yoder and Ruth Signorell*

1. Correction of measured cluster size distributions to account for cluster size-dependent EUV photoionization cross sections

The cluster size distributions were measured with the Na-doping method after UV ionization of Na-doped clusters, while the photoelectron spectra were recorded after EUV ionization of the clusters (see section 2 in the main text). As explained below, the ionization cross sections of the Na-doping method ($\sigma(n)_{UV,Na}$) and EUV ionization ($\sigma(n)_{EUV}$) have different cluster size dependences. Therefore, the cluster size distribution measured with the Na-doping method needs to be corrected to account for the different cluster size dependence of the EUV photoionization cross section.

We assume that the cross section for single photon EUV ionization of a water cluster $\sigma(n)_{EUV}$ is proportional to the number of molecules *n* in the cluster:

$$\sigma(n)_{EUV} \propto n. \qquad \text{Eq. S 1}$$

For the single photon UV ionization of a Na-doped cluster, the ionization cross section is proportional to the average number of Na atoms $\langle m(n)\rangle$ in the cluster of *n* water molecules:

$$\sigma(n)_{UV,Na} \propto \langle m\,(n)\rangle. \qquad \text{Eq. S 2}$$

The pick-up of Na atoms by water clusters traversing our Na-oven is governed by Poisson collision statistics. The calculation of pick-up probability $p(m,n)$ of m atoms by clusters composed of n monomer units has been described in refs. [1, 2]. We assume hard sphere cross sections and sticking coefficients of unity, i.e. every collision leads to the capture of a Na atom. The latter is a reasonable assumption except for the smallest clusters, which are not considered in this work. From $p(m,n)$ it is now possible to calculate

$$\langle m(n)\rangle = \sum_m mp(m,n)\,, \qquad \text{Eq. S 3}$$

A detailed analysis shows that for our setup

$$\langle m\,(n)\rangle \propto n^{0.63}. \qquad \text{Eq. S 4}$$

To account for the EUV size-dependent ionization cross sections, the intensities in the size distributions measured with the Na-doping method need to be corrected by the size-dependent factor

$$\sigma_{VUV}/\sigma_{UV,Na} = n/n^{0.63} = n^{0.37}. \qquad \text{Eq. S 5}$$

2. Scattering cross sections for models (i) to (iv)

Fig. S1, S2, and S3 show the scattering cross sections for quasi-elastic (elastic and phonon), vibron, and electronic scattering, respectively, for the four different cases (i)-(iv) defined in section 3 of the main text.

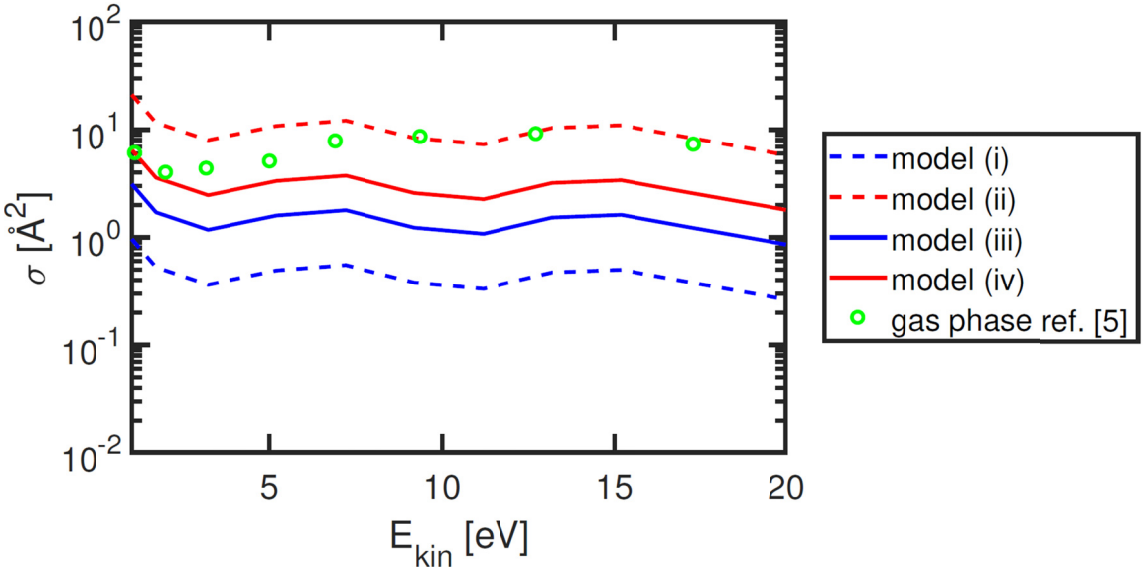

Figure S1: Electron scattering cross sections for quasi-elastic processes.

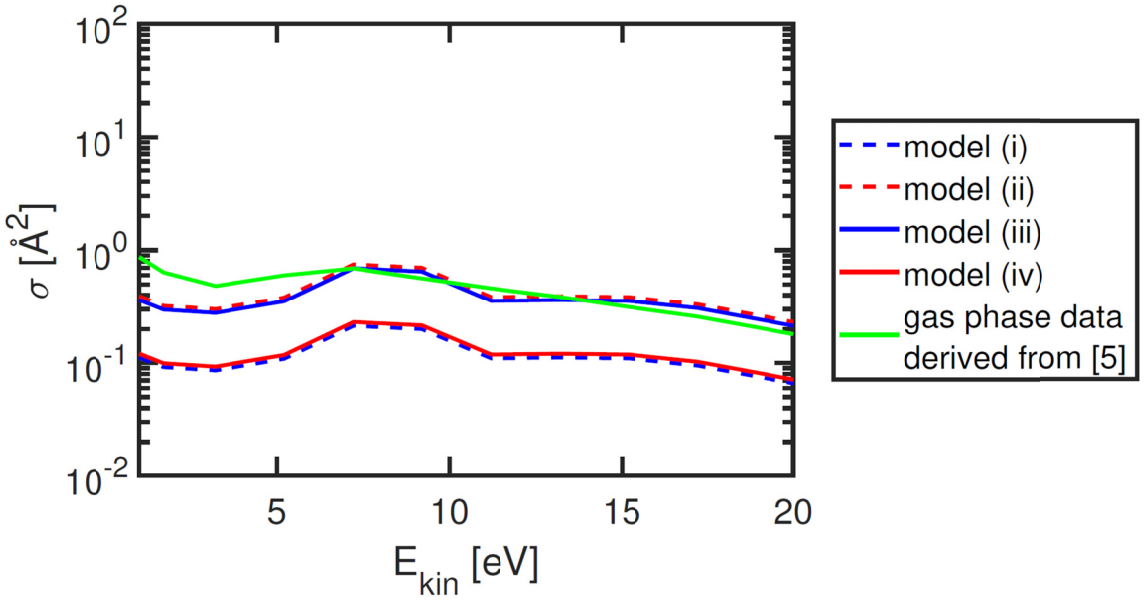

Figure S2: Electron scattering cross sections for scattering by vibrational modes.

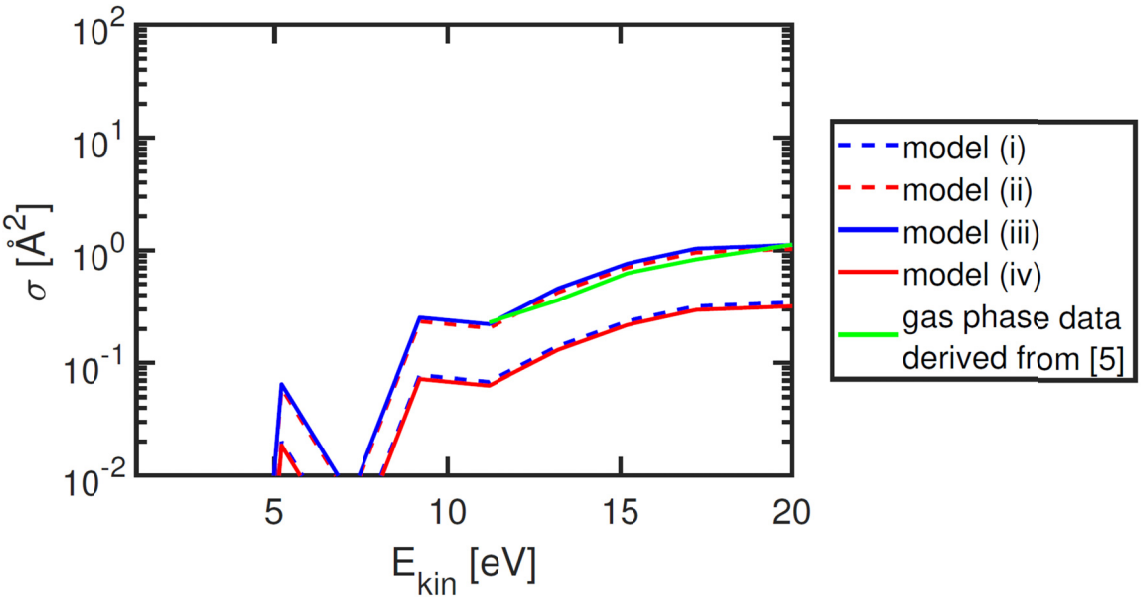

Figure S3: Electron scattering cross sections for scattering by electronic modes.

To mimic gas phase scattering (model (ii); dashed red lines), the condensed bulk phase scattering cross sections of model (i) (dashed blue lines)[3, 4] were scaled with constant scaling factors to match the corresponding gas phase data recommended by Itikawa and Mason (green circles and full green lines)[5]. The scaling factors for quasi-elastic, vibron, and electronic scattering are 22, 3.5, and 3, respectively. The scaling factors for each class of processes were determined to give reasonable agreement in the energy range between 5 and 15 eV. For the quasi-elastic processes (Fig. S1), the sum of the condensed phase elastic scattering cross sections and the isotropic parts of all condensed phase phonon scattering cross sections was scaled to match the gas phase momentum transfer cross sections given by Itikawa and Mason[5]. For the vibrational excitations (Fig. S2), the sum of all condensed phase vibrational cross sections [3, 4] was scaled to the sum of all gas phase vibrational cross sections [5]. In order to sum the gas phase vibrational cross sections the discrete data points were first linearly interpolated. For the electronic excitations (Fig. S3), the total condensed phase electronic cross sections [3, 4] were scaled to match the sum of the total gas phase ionization cross section and the gas phase cross section for dissociation into OH[5]. To perform the summation of the two gas phase data sets, the discrete data points were first linearly interpolated.

To exclude the effect of dielectric screening in the condensed phase (model (iii), full blue lines), all condensed phase cross sections of model (i) were scaled by a factor of 3.24. Similarly, to include the effect of dielectric screening to the gas phase (model (iv), full red lines), all gas phase cross section of model (ii) were scaled by a factor of 1/3.24

3. Determination of electron binding energy shifts

Electron binding energy shifts $\Delta eBE = |eBE(c) - eBE(m)|$ were determined as the absolute difference of the water monomer binding energy $eBE(m)$ and the cluster binding energy $eBE(c)$. The cluster binding energies were determined by fitting a sum of Gaussian peaks to the binding energy spectra. The $1b_1$ and $1b_2$ bands were represented by single Gaussian peaks, while the $3a_1$ band was fitted

using two Gaussian peaks of equal intensity. For the $3a_1$ band, the average of the two peak positions was considered as binding energy. Then uncertainties of the absolute value of ΔeBE is estimated to be <100 meV for the $1b_1$ band and <200 meV for the $1b_2$ band. For the $3a_1$ band the uncertainty is slightly higher at ~250 meV, due to some remaining ambiguity in the monomer subtraction and the fitting of the double Gaussian peak shape. We expect that the uncertainty of the relative change of ΔeBE as a function of cluster size is significantly smaller as it is indicated by the spread of the actual data points (Fig. 3 main text). In addition, peak widths (Full Width at Half Maximum: FWHM) were also determined from the fits. The estimated uncertainties in the FWHM are <200 meV for the $1b_1$ and $1b_2$ bands and ~300 meV for the $3a_1$ band. ΔeBE shifts and FWHMs are only reported for the cases for which the signal levels were high enough to perform the monomer subtraction prior to fitting the spectra.

Table S1: Binding energy shifts ΔeBE and peak widths (FWHM) for different average cluster sizes $< n >$.

	$1b_1$		$3a_1$		$1b_2$	
$< n >$	ΔeBE [eV]	FWHM [eV]	ΔeBE [eV]	FWHM [eV]	ΔeBE [eV]	FWHM [eV]
43	0.69	1.55	0.70	3.15	0.58	2.56
59	0.69	1.57	0.49	2.08	0.91	2.10
60	0.79	1.65	0.62	2.92	0.81	2.48
65	0.81	1.43	0.62	2.68	0.91	2.25
70	0.87	1.21	0.85	3.33	0.87	2.27
81	0.68	1.84	0.41	2.30	0.88	2.37
88	0.84	1.53	0.70	2.91	0.86	2.55
104	0.84	1.49	0.67	2.87	0.75	2.63
106	0.84	1.48	0.77	2.85	0.92	2.38
111	0.85	1.73	0.72	2.96	0.79	2.58
117	0.90	1.48	0.76	2.87	0.91	2.47
117	0.91	1.45	0.77	2.93	0.91	2.33
118	0.88	1.29	0.98	2.84	0.85	1.91
124	0.94	1.49	0.77	2.91	0.74	2.69
135	0.90	1.44	0.80	2.98	0.91	2.45
142	0.87	1.42	0.84	3.15	0.88	2.33
144	0.97	1.55	0.76	2.66	0.95	2.53
157	0.94	1.38	0.85	2.88	0.78	2.64
166	1.03	1.48	0.92	2.79	0.99	2.79
178	0.95	1.36	0.77	3.12	0.91	2.59
193	0.92	1.30	0.83	2.87	0.90	2.39
195	0.95	1.61	0.79	2.79	0.97	2.61
204	1.00	1.52	0.91	3.18	0.88	2.79
210	1.01	1.54	0.93	3.23	0.85	2.89
219	1.04	1.52	0.92	2.92	0.92	2.80
219	1.04	1.52	0.91	2.90	0.94	2.77
227	0.97	1.50	0.81	2.94	0.78	2.86
239	0.99	1.51	0.88	3.09	0.76	2.88
246	0.97	1.62	0.77	2.74	0.88	2.72
251	1.01	1.59	0.95	3.22	0.82	2.80
251	1.00	1.47	0.88	3.03	0.81	2.66
251	1.02	1.58	0.84	2.84	0.91	2.78
254	1.02	1.51	0.88	2.98	0.89	2.82
266	0.97	1.28	0.83	2.92	0.97	2.67

274	1.02	1.51	0.91	3.02	0.89	2.78
292	1.08	1.45	0.90	3.02	0.82	2.91
297	1.04	1.58	0.86	2.73	0.94	2.83
299	1.01	1.43	0.83	3.04	0.86	2.61
315	1.02	1.32	0.86	3.11	0.87	2.57
336	1.09	1.51	0.99	2.62	0.87	2.98
343	1.06	1.58	0.92	2.91	0.86	3.01
351	1.08	1.55	0.91	2.89	0.88	2.99
355	1.11	1.52	1.01	3.11	0.79	3.08
361	1.03	1.56	0.90	2.98	0.79	2.97
382	0.99	1.35	0.83	2.85	0.99	2.66
388	1.10	1.56	1.00	2.94	0.83	3.31
388	1.09	1.55	0.96	2.96	0.83	3.03
395	1.11	1.46	0.99	2.67	0.98	2.73
405	1.01	1.40	0.80	3.00	0.92	2.60
417	0.99	1.37	0.77	3.03	0.87	2.71
471	1.05	1.72	0.91	3.06	0.67	3.38
499	1.01	1.32	0.78	3.02	0.89	2.75
503	1.03	1.42	0.85	2.93	1.00	2.81
528	1.01	1.41	0.80	2.88	0.99	2.87
561	1.03	1.63	0.93	3.14	0.68	3.25
583	1.10	1.38	1.02	3.22	0.59	3.46
611	1.00	1.44	0.79	2.82	1.09	2.83
671	1.10	1.35	1.02	3.36	0.56	3.38

4. Determination of β parameters

β parameters were determined as the average over ~80% of the bands' FWHM to reduce contributions from regions where the bands overlap (see Fig. 2b in the main text) and from regions of low signal. The retrieved experimental β parameters are listed in Table S2 and shown in Fig. 4 in the main text and in Figs. S4 and S5 below. The uncertainties given in brackets in Table S2 and shown as error bars in the figures correspond to one standard deviation of the β traces over the range given by ~80% of the peaks FWHM. For spectra for which the signal level was too low to perform an unambiguous monomer subtraction, we were only able to retrieve reliable β values for the $1b_1$ band.

Table S2: Experimental β parameters as a function of cluster size $< n >$ for photoionization from the three valence orbitals of water with EUV photons of 26.5, 20.3 and 14.0 eV radiation.

$h\nu$ =26.5 eV	β		
$< n >$	$1b_1$	$3a_1$	$1b_2$
43	0.72(18)	0.53(59)	0.27(47)
59	0.67(22)	0.12(31)	0.32(39)
60	0.63(10)	0.30(23)	0.24(18)
65	0.60(16)	0.26(41)	0.33(33)
81	0.64(13)	0.33(17)	0.34(16)
88	0.57(13)	0.25(21)	0.28(22)
104	0.53(14)	0.27(16)	0.22(18)
106	0.64(6)	0.37(15)	0.36(12)
111	0.39(7)	0.23(15)	0.24(13)
117	0.53(16)	0.21(31)	0.29(26)
117	0.54(16)	0.16(18)	0.28(26)
118	0.70(29)	0.24(75)	0.31(38)
135	0.56(13)	0.20(17)	0.34(22)
142	0.62(12)	0.27(13)	0.39(11)
144	0.50(14)	0.22(11)	0.24(19)
166	0.45(17)	0.10(19)	0.23(20)
195	0.42(4)	0.12(8)	0.25(17)
204	0.46(8)	0.16(9)	0.20(14)
210	0.43(10)	0.13(17)	0.13(17)
219	0.44(14)	0.17(6)	0.20(16)
219	0.42(15)	0.17(5)	0.21(15)
227	0.42(15)	0.20(6)	0.18(14)
239	0.37(5)	0.16(7)	0.09(13)
251	0.44(8)	0.01(17)	0.22(18)
251	0.42(8)	0.18(8)	0.17(14)
251	0.40(14)	0.15(7)	0.17(15)
254	0.43(6)	0.17(13)	0.21(15)
274	0.44(7)	0.19(12)	0.22(16)
292	0.39(13)	0.22(12)	0.20(14)
297	0.38(15)	0.11(11)	0.16(14)
336	0.34(9)	0.03(24)	0.18(17)
343	0.32(7)	0.14(6)	0.19(11)
351	0.35(15)	0.13(6)	0.14(12)

355	0.35(9)	0.19(21)	0.12(16)
361	0.36(4)	0.18(9)	0.15(11)
388	0.29(7)	0.12(7)	0.16(14)
388	0.27(9)	0.09(9)	0.14(14)
395	0.32(19)	-0.08(10)	0.07(14)
471	0.34(5)	0.17(6)	0.09(12)
561	0.34(6)	0.15(7)	0.10(12)
583	0.31(17)	0.16(5)	0.11(12)
671	0.28(18)	0.08(5)	0.05(11)
$h\nu$ =20.3 eV		β	
$< n >$	$1b_1$	$3a_1$	$1b_2$
51	0.51(11)		
53	0.47(21)		
70	0.48(26)		
91	0.45(12)		
111	0.36(8)		
119	0.47(16)		
123	0.35(14)		
124	0.25(12)	0.11(12)	-0.05(14)
157	0.34(7)	0.06(21)	-0.06(14)
178	0.29(20)		
193	0.33(9)	0.03(20)	-0.03(13)
246	0.26(12)	0.05(19)	-0.05(17)
266	0.29(7)	0.02(13)	-0.05(8)
299	0.23(8)	0.08(9)	-0.05(7)
315	0.26(10)	0.09(10)	-0.04(11)
382	0.25(8)	0.03(13)	-0.04(8)
405	0.23(8)	0.04(8)	-0.04(8)
417	0.23(9)	0.06(10)	-0.04(7)
499	0.23(9)	0.06(12)	-0.05(10)
503	0.22(7)	0.07(10)	-0.05(8)
528	0.23(9)	0.04(11)	-0.05(8)
611	0.25(9)	0.06(12)	-0.03(10)
$h\nu$ =14.0 eV		β	
$< n >$	$1b_1$	$3a_1$	$1b_2$
44	0.08(29)		
63	0.02(23)		
69	0.05(26)		
181	-0.01(18)		
232	0.00(10)		
319	-0.01(8)		
360	-0.02(6)		
477	-0.03(6)		

Figs. S4 and S5 show the β parameters from Table S2 for the $3a_1$ and the $1b_2$ band, respectively. The corresponding data for the $1b_1$ band is shown in Fig. 4 in the main text. The calculated liquid jet values are corrected for the polarization dependent coupling of the laser light into the jet. Laser light polarized along the jet axis couples slightly less effectively into the liquid than light polarized perpendicular to it (i.e. parallel to the detector in the usual arrangement). This leads to a slightly higher photoelectron current for the latter polarization compared with the former and thus a slightly higher (more positive) apparent β value. In our calculations we correct for this effect by normalizing the photoelectron currents to the field strength inside the liquid jet.

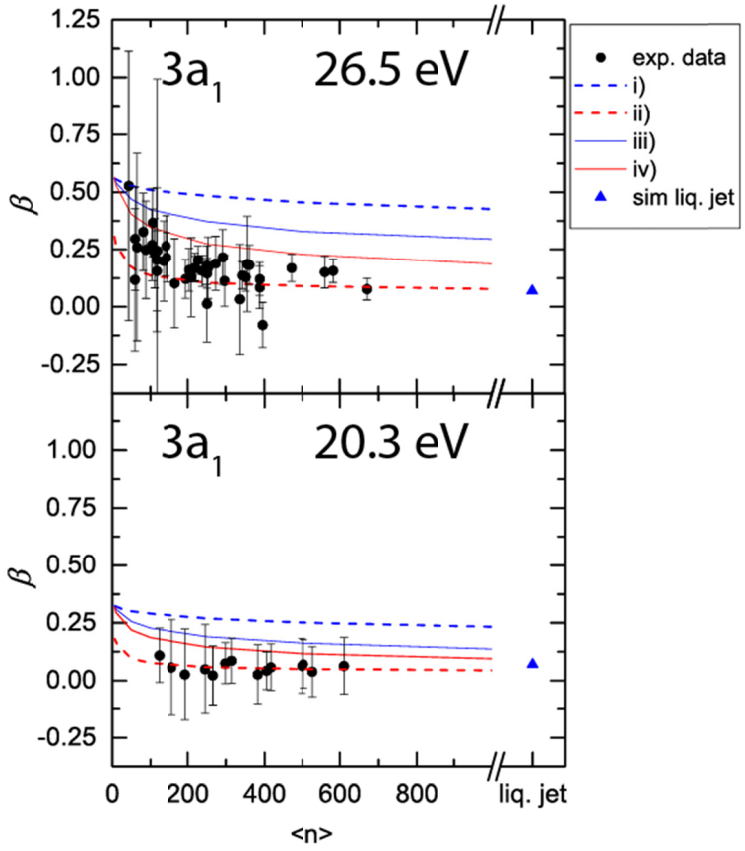

Figure S4: β parameters as a function of cluster size $\langle n \rangle$ for photoionization from the $3a_1$ orbital using HH radiation of $h\nu$ = 26.5 eV (top) and 20.3 eV (bottom). Black circles: experimental data. Dashed blue lines: simulation with model (i). Dashed red lines: simulation with model (ii). Full blue lines: simulation with model (iii). Full red lines: simulation with model (iv). Blue triangles: prediction for liquid jet (corrected for the polarization dependent coupling of the laser light) using the scattering parameters from model (i).

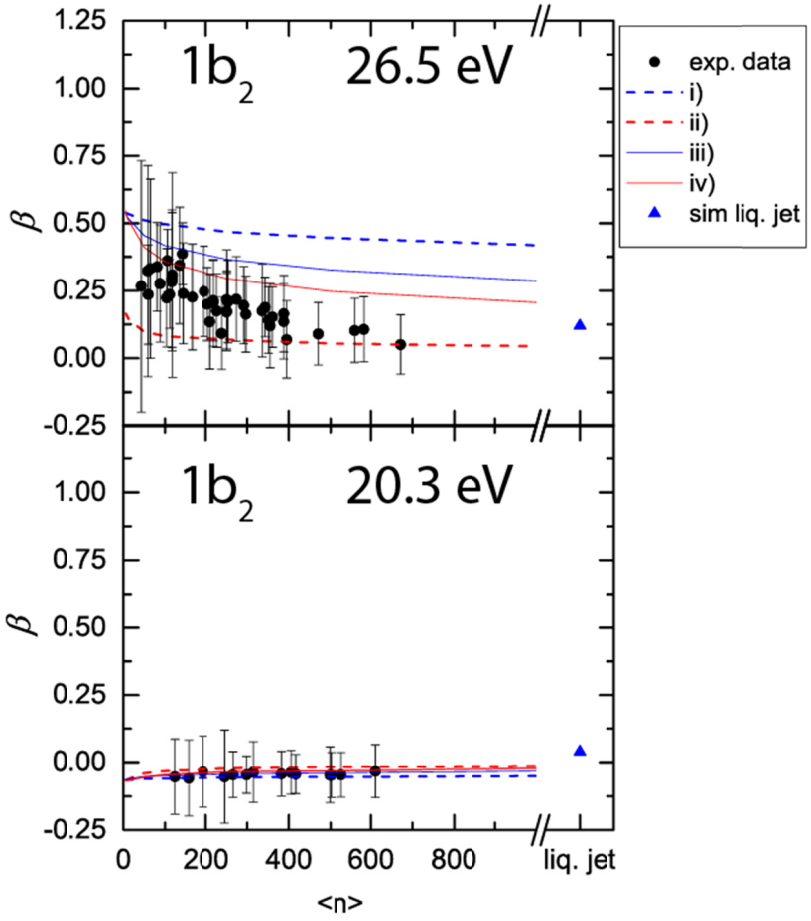

Figure S5: β parameters as a function of cluster size $\langle n \rangle$ for photoionization from the $1b_2$ orbital using HH radiation of $h\nu$ = 26.5 eV (top) and 20.3 eV (bottom). Black circles: experimental data. Dashed blue lines: simulation with model (i). Dashed red lines: simulation with model (ii). Full blue lines: simulation with model (iii). Full red lines: simulation with model (iv). Blue triangles: prediction for liquid jet using the scattering parameters from model (i). Note the different ordering of models for the $1b_2$ band at 20.3 eV because β_{inp} is slightly negative. The corresponding calculated liquid jet value remains very slightly positive because of the contribution of inelastically scattered electrons originating from the $1b_1$ and $3a_1$ orbitals.

5. Calculation of photoelectron images for bimodal cluster size distributions with a small and a large mode; Explanation of shadowing in photoelectron images

Section 4.2 and Table 1 in the main text discuss the influence of bimodal cluster size distributions with a small and a large mode on the β parameter and on the photoelectron images (shadowing). The following paragraphs explain how the corresponding photoelectron images and β parameters (β_{calc}) were calculated and exemplify the term "shadowing".

The bimodal size distributions consist of a small percentage p_{large} of very large clusters of size n_{large}=5 × 10^4, 10^5, 2.5 × 10^5, or 5 × 10^5 and a large percentage $p_{\langle n \rangle}$ of clusters of $n=\langle n \rangle$=500 molecules. The simulated photoelectron images Im were calculated as a weighted sum of the simulated photoelectron image $\mathrm{Im}(\langle n \rangle)$ for $\langle n \rangle$=500 and the simulated photoelectron image $\mathrm{Im}(n_{large})$ for n_{large}

$$\mathrm{Im} = p_{\langle n \rangle} \cdot \mathrm{Im}(\langle n \rangle) + p_{large} \cdot \mathrm{Im}(n_{large}) \qquad \text{Eq. S 6}$$

The resulting image Im was reconstructed and β_{calc} was determined in the same way as β_{exp} from the experimental images (see section 4 above).

Shadowing is an effect occurring in photoemission from larger clusters and aerosol particles due to stronger absorption of the ionizing radiation on the side of the cluster/particle where the light impinges on the cluster/particle[6]. As an example Fig. 6 shows the calculated light intensity inside a particle for incident EUV light. The light intensity in the particle drops along the light propagation direction because of light absorption.

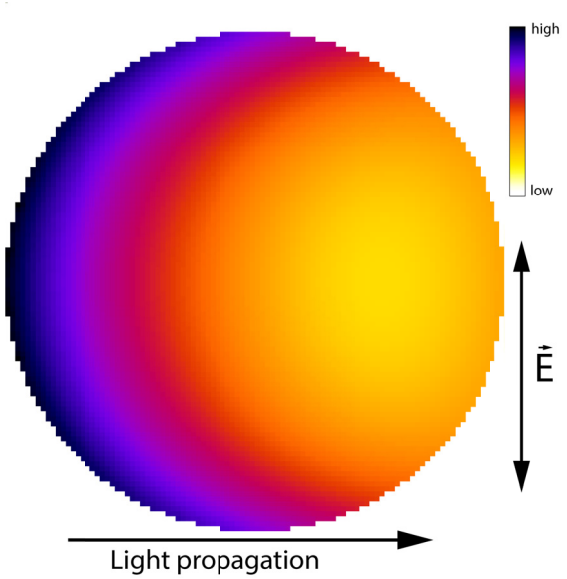

Figure S6: Calculated light intensity distribution in the equatorial plane of a water particle using an FDTD approach. Black is high and yellow is low light intensity.

The inhomogeneous illumination inside the particle causes more unbound electrons to be born in the particle hemisphere where the ionizing radiation impinges (left side in Fig. S6). This leads to the ejection of more photoelectrons in this region and thus to a correspondingly inhomogeneous photoelectron image as shown in Fig. 7. This effect is referred to as shadowing. We quantify the degree of shadowing in photoelectron images by a parameter α, which is defined as the ratio of photoelectron counts detected in the "backward" and "forward" halves of an photoelectron image (Fig. 7):

$$\alpha = I_{\mathrm{backward}} / I_{\mathrm{forward}} \qquad \text{Eq. S 7}$$

α = 1 for a homogeneous photoelectron image and α > 1 when shadowing occurs (Fig. 7). Images with α > 1.1 (i.e. one half of the electron image has 10% more intensity than the other) show clear shadowing. These cases are labeled in Table 1 in the main text as "shadowing: yes", while cases with 1 ≤ α ≤ 1.1 are labeled as "shadowing: no". Note that none of our experimental spectra shows any detectable shadowing, i.e. all experiments yield α ≤ 1.1.

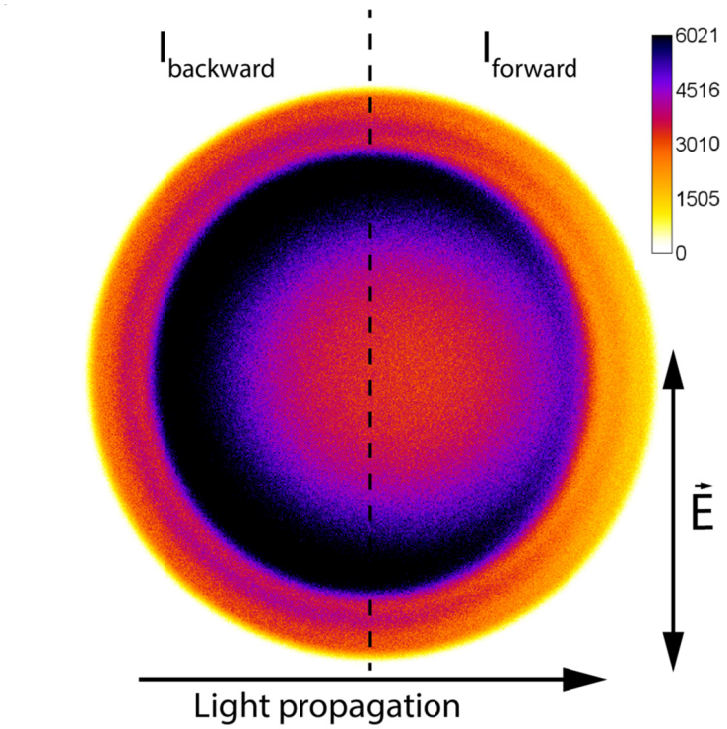

Figure S7: Simulated raw photoelectron image of a water particles showing shadowing (α =1.26). Black is high and yellow is low electron intensity.

References

1. B. Schläppi, J. J. Ferreiro, J. H. Litman and R. Signorell, Int. J. Mass Spectrom. **372**, 13-21 (2014).
2. S. Vongehr, S.-C. Tang and X.-K. Meng, Chinese Physics B **19** (2) (2010).
3. M. Michaud, A. Wen and L. Sanche, Radiat. Res. **159** (1), 3-22 (2003).
4. R. Signorell, M. Goldmann, B. L. Yoder, A. Bodi, E. Chasovskikh, L. Lang and D. Luckhaus, Chem. Phys. Lett. **658**, 1-6 (2016). D. Luckhaus, Y. I. Yamamoto, T. Suzuki and R. Signorell, *Science Advances*, 2017, **3**, e1603224.
5. Y. Itikawa and N. Mason, Journal of Physical and Chemical Reference Data **34** (1), 1-22 (2005).
6. M. Goldmann, J. Miguel-Sanchez, A. H. C. West, B. L. Yoder and R. Signorell, J. Chem. Phys. **142** (22), 8 (2015).